OXFORD

Cerebral Cortex, 2023, **33**, 10686–10701
https://doi.org/10.1093/cercor/bhad318
Advance access publication date 8 September 2023
Original Article

Hierarchical organization of the human ventral visual streams revealed with magnetoencephalography

Edmund T. Rolls [1,2,3,*], Gustavo Deco[4,5,6], Yi Zhang[3], Jianfeng Feng[2,3]

[1]Oxford Centre for Computational Neuroscience, Oxford, United Kingdom,
[2]Department of Computer Science, University of Warwick, Coventry CV4 7AL, United Kingdom,
[3]Institute of Science and Technology for Brain Inspired Intelligence, Fudan University, Shanghai 200403, China,
[4]Center for Brain and Cognition, Computational Neuroscience Group, Department of Information and Communication Technologies, Universitat Pompeu Fabra, Roc Boronat 138, Barcelona 08018, Spain,
[5]Brain and Cognition, Pompeu Fabra University, Barcelona 08018, Spain,
[6]Institució Catalana de la Recerca i Estudis Avançats (ICREA), Universitat Pompeu Fabra, Passeig Lluís Companys 23, Barcelona 08010, Spain

*Corresponding author: Department of Computer Science, University of Warwick, Coventry CV4 7AL, United Kingdom. Email: Edmund.Rolls@oxcns.org

The hierarchical organization between 25 ventral stream visual cortical regions and 180 cortical regions was measured with magnetoencephalography using the Human Connectome Project Multimodal Parcellation atlas in 83 Human Connectome Project participants performing a visual memory task. The aim was to reveal the hierarchical organization using a whole-brain model based on generative effective connectivity with this fast neuroimaging method. V1–V4 formed a first group of interconnected regions. Especially V4 had connectivity to a ventrolateral visual stream: V8, the fusiform face cortex, and posterior inferior temporal cortex PIT. These regions in turn had effectivity connectivity to inferior temporal cortex visual regions TE2p and TE1p. TE2p and TE1p then have connectivity to anterior temporal lobe regions TE1a, TE1m, TE2a, and TGv, which are multimodal. In a ventromedial visual stream, V1–V4 connect to ventromedial regions VMV1–3 and VVC. VMV1–3 and VVC connect to the medial parahippocampal gyrus PHA1–3, which, with the VMV regions, include the parahippocampal scene area. The medial parahippocampal PHA1–3 regions have connectivity to the hippocampal system regions the perirhinal cortex, entorhinal cortex, and hippocampus. These effective connectivities of two ventral visual cortical streams measured with magnetoencephalography provide support to the hierarchical organization of brain systems measured with fMRI, and new evidence on directionality.

Key words: visual cortical streams; humans; effective connectivity using MEG; hippocampus; inferior temporal visual cortex.

Introduction

Magnetoencephalography (MEG) is a fast neuroimaging modality with a high temporal resolution of ms that has the potential to complement fMRI by providing evidence on the flow of information through the brain. When combined with measures of whole-brain model based effective connectivity (EC), MEG has the potential to reveal the flow of information though different brain systems, and thus the hierarchical organization. EC measures correlations between the signals measured with short delays between brain regions, and then can use a whole-brain Hopf model of the delayed interactions between cortical regions to produce what is termed a generative EC matrix, in that it can generate the functional connectivities and the delayed functional connectivities (Deco et al. 2017b, 2019; Rolls et al. 2022b) as described in the Methods. The analysis of EC with fMRI data does provide a real complement to analysis with MEG data, as the fMRI data have better spatial resolution, though poorer temporal resolution than MEG. It is highly relevant that the characteristic timescale for the operation of a cortical region is approximately 15 ms (Wallis and Rolls 1997; Rolls 2023a), which is the time that it takes for the recurrent collaterals between nearby pyramidal cells to be used in local attractor dynamics (Panzeri et al. 2001; Rolls 2016, 2023a), so an analysis with MEG that can provide data on the scale of 10 ms or better is appropriate and potentially very useful.

In the present investigation, the generative EC of human ventral visual system cortical regions was investigated with MEG, and there is extensive task-related MEG data available from the Human Connectome Project (HCP) using visual stimuli (Larson-Prior et al. 2013). Data from four visual tasks were analyzed here, in which faces and tools were used as stimuli, and which included 0-back and 2-back memory tasks for the visual stimuli (see Methods). The MEG analyses of task-related data described here are intended to complement the analysis of human visual pathways performed with resting-state fMRI, with the especial aim of using the MEG analysis to provide more direct evidence on the directionality of the EC. In the previous analysis with resting-state fMRI, several visual cortical streams were identified (Rolls et al. 2023c). These streams included a Ventrolateral Visual "What" Stream for object and face recognition that projects hierarchically to the inferior temporal visual cortex which projects to the hippocampal memory system (Rolls 2021, 2023a; Rolls et al. 2023c). A Ventromedial Visual "Where" Stream for scene representations connects to the parahippocampal gyrus and hippocampus (Rolls 2023a, 2023c, 2023d; Rolls et al. 2023c). The improving understanding of the connectivity of

Received: June 8, 2023. **Revised:** August 17, 2023. **Accepted:** August 17, 2023

the visual streams with the human hippocampus is helping to revolutionize our understanding of the visual "what" (faces and objects) and "where" (viewed spatial scenes) inputs to the human hippocampus, and is leading to fundamental advances in our understanding of human and non-human primate hippocampal function in episodic memory (Rolls 2023a, 2023c, 2023d). Partly for these reasons, it is important to understand better the ventral stream visual pathways in humans, and that is a key rationale to utilize the fast neuroimaging method MEG to analyze these pathways in humans as described here.

In the present analyses using MEG data, the EC of visual cortical regions from these ventral streams to the hippocampal system was investigated, because the task-related data involved visual stimuli such as faces and tools that are processed in the ventral visual system, and because the MEG data included n-back memory tasks of the type that utilize hippocampal system regions such as the perirhinal cortex (Baxter and Murray 2001a, 2001b; Buckley and Gaffan 2006). The effective connectivities were measured between ventral stream visual cortical regions in the Human Connectome Project Multimodal Parcellation Atlas (HCP-MMP; Glasser et al. 2016). The HCP-MMP atlas provides the most detailed parcellation of the human cortical areas that we know, in that its 360 regions are defined using a combination of structural measures (cortical thickness and cortical myelin content), functional connectivity, and task-related fMRI (Glasser et al. 2016). This parcellation is the parcellation of choice for the cerebral cortex because it is based on multimodal information (Glasser et al. 2016) with the definition and boundaries set out in their Glasser_2016_SuppNeuroanatomy.pdf, and it is being used as the basis for many new investigations of brain function and connectivity, which can all be cast in the same framework (Colclough et al. 2017; Van Essen and Glasser 2018; Sulpizio et al. 2020; Yokoyama et al. 2021; Ma et al. 2022; Rolls et al. 2022a, 2022b, 2023b, 2023c, 2023d, 2023e, 2023f; Rolls 2023a; Rolls et al. 2023i; Rolls et al. 2023j). A summary of the boundaries, tractography, functional connectivity and task-related activations of visual cortical areas using the HCP-MMP atlas is available elsewhere (Glasser et al. 2016; Baker et al. 2018a, 2018b), but the effective and functional connectivity measures described here are new, in that they are based on visual task-related MEG data.

Methods

Magnetoencephalographic data analyzed

The MEG data that were analyzed were collected and preprocessed by the HCP, which provides full details (Larson-Prior et al. 2013). The data were for 83 participants performing a visual working memory task in which visual stimuli (faces, and tools) were presented in a 0-back and 2-back task with 2 s for each stimulus. For each task, a timeseries with 91 points spaced 20 ms apart was provided by the HCP in which the visual stimulus was shown in timebin 31. (Data were also available for the resting state in 89 participants, with typically 14,000 points in a timeseries spaced after preprocessing 20 ms apart.)

The MEG data were pre-processed by the HCP consortium (Larson-Prior et al. 2013). All the data were first run through the quality assessment procedure. Bad channels, which were dissimilar to their neighbors, and bad segments identified by iterative independent component analysis (ICA), were removed. ICA was then used to remove physiological artifacts and environmental noises, including electrocardiogram, eye movements, power supply bursting, etc.

The MEG signal in sensor space was further localized into the surface-based source space during the HCP preprocessing. Weighted minimum-norm estimates were used to reconstruct the source space for resting-state MEG scans from structural MRI, and linear constrained minimum variance beamformers were used to reconstruct the source space for task MEG scans. Details can be found in Larson-Prior et al. (2013).

We then converted the MEG data provided by the HCP with a 20 ms time scale into the HCP-MMP1 surface space (Glasser et al. 2016) as follows. The vertex-based template for the multi-modal parcellation (mmp) was first resliced from 32 to 4 k using the HCP workbench command-line tool (–label-resample) to match the spatial resolution of the source reconstructed MEG data. The time series for vertices within each of the 360 cortical regions in the HCP-MMP1 atlas were then averaged to produce a 20 ms MEG timeseries in HCP-MMP1 space for each participant. Although the spatial resolution of the MEG data may not be sufficient to provide an independent signal for each of the 360 cortical regions in the HCP-MMP atlas, the use of the atlas is potentially valuable because the cortical regions in the atlas are themselves well-defined (Glasser et al. 2016), and use of this atlas provides a framework for comparing findings from different investigations of the cortex (Sulpizio et al. 2020; Wan et al. 2022; Rolls 2023a, 2023b; Rolls et al. 2022a, 2022b, 2023a, 2023b, 2023c, 2023d, 2023e, 2023f, 2023g, 2023h, 2023i, 2023j; Zhang et al. 2023). It is noted that the spatial resolution of MEG may be poorer for visual cortical regions far from the skull, due to the inverse problem, and also that this is unlikely to account for the findings described here, in that many regions high in the hierarchy such as the TE regions are as close to the skull as early visual cortical regions (see Figs. S1–S5).

The EC between the 360 cortical regions was computed with the same Hopf connectivity approach used for the fMRI data (Rolls et al. 2023c). Because the MEG timeseries could be very long, the EC was calculated with an analytic version of the Hopf algorithm, instead of the simulation approach used for fMRI data (Rolls et al. 2023c). The analytic approach is described in the Supplementary Material, and when tested with fMRI data, produced very similar results to the simulation approach ($r > 0.95$ for a comparison of the effective connectivities calculated with the simulation and analytic methods).

Brain atlas and region selection

To construct the EC for the regions of interest in this investigation with other parts of the human brain, we utilized the parcellation of human cortical regions provided in the HCP-MMP1, which has 360 cortical regions (Glasser et al. 2016). The brain regions in this atlas (Glasser et al. 2016) are shown in Fig. 1 and Fig. S1, and a list of the cortical regions in this atlas and the divisions into which they are placed is provided in Table S1 in the reordered form used in the extended volumetric HCPex atlas (Huang et al. 2022).

The 25 ventral visual cortical regions selected for connectivity analysis here were as follows, with reference to Fig. 1 useful in showing where these regions are in the human brain. The regions are grouped based on earlier evidence (Glasser et al. 2016; Rolls et al. 2023c) purely to simplify the description of the connectivity, and the groups are separated by red lines in Figs. 3–6:

Group 1: Early Visual cortical areas V1, V2 and V4 of the HCP-MMP atlas.

Group 2: intermediate cortical visual regions FFC (fusiform face cortex), PIT (posterior inferior temporal), and V8.

Group 3: medial temporal lobe visual regions with connectivity with the hippocampus. This group includes posterior ventromedial visual regions VMV1–3 and VVC; the medial

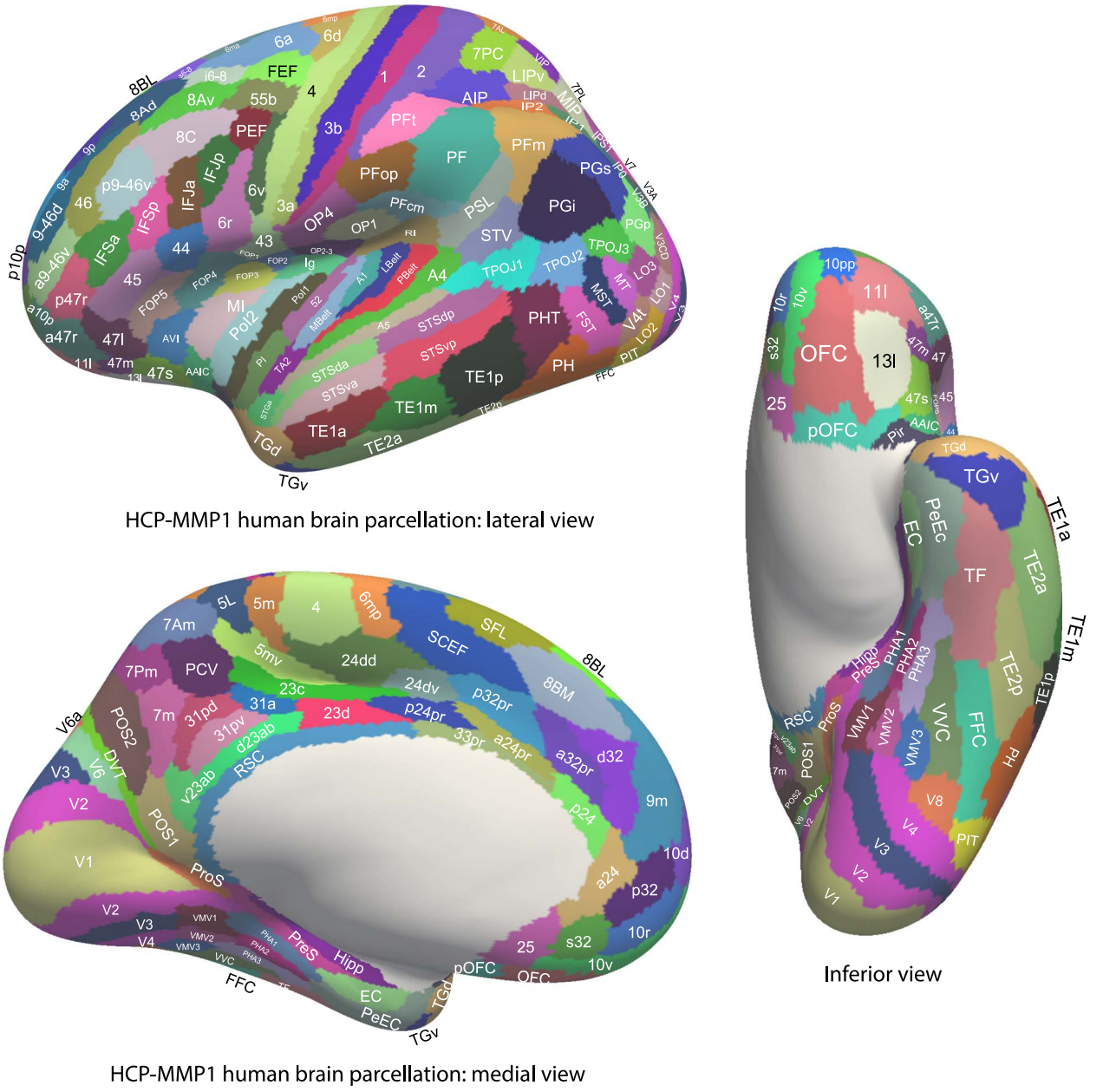

Fig. 1. Regions in the Human Connectome Project Multimodal Parcellation atlas (HCP-MMP) (Glasser et al. 2016) and its extended version HCPex (Huang et al. 2022) to show the cortical regions. The regions are shown on images of the human brain with the sulci expanded sufficiently to allow the regions within the sulci to be shown. Abbreviations are provided in Table S1. For comparison, a version of this diagram without the sulci expanded is provided in Figs. S1–S5.

parahippocampal cortex PHA1–3; the lateral parahippocampal cortex TF; the perirhinal cortex PeEc, the entorhinal cortex EC, the presubiculum PreS, and the hippocampus Hipp. The parahippocampal scene area (or parahippocampal place area (Rolls 2023c, 2023d)) is at the junction of VMV1–3 and PHA1–3 in the medial parahippocampal gyrus (Sulpizio et al. 2020).

Group 4: Inferior temporal visual cortex regions TE2p and TE1p.

Group 5: Multimodal cortical regions in the anterior temporal lobe TE1a, TE1m, TE2a; and temporal pole regions TGd and TGv.

Measurement of EC

EC measures the effect of one brain region on another, and utilizes differences detected at different times in the signals in each connected pair of brain regions to infer effects of one brain region on another. One such approach is dynamic causal modeling, but it applies most easily to activation studies, and is typically limited to measuring the EC between just a few brain areas (Friston 2009; Valdes-Sosa et al. 2011; Bajaj et al. 2016), though there have been moves to extend it to resting-state studies and more brain areas (Frassle et al. 2017; Razi et al. 2017). The method used here (see Rolls et al. 2022b, 2023d) was developed from a Hopf algorithm to enable measurement of EC between many brain areas, described by Deco et al. (2019). A principle is that the functional connectivity is measured at time t and time $t + tau$, where tau was set to 20 ms, which is the timescale available with the HCP MEG data.

To infer the EC, we use a whole-brain model that allows us to analyze the MEG signal across all brain regions and time. We use the so-called Hopf computational model, which integrates the dynamics of Stuart–Landau oscillators, expressing the activity of each brain region, by the underlying anatomical connectivity

(Deco et al. 2017b). As mentioned above, we include in the model 360 cortical brain areas (Huang et al. 2022). The local dynamics of each brain area (node) is given by Stuart–Landau oscillators, which expresses the normal form of a supercritical Hopf bifurcation, describing the transition from noisy to oscillatory dynamics (Kuznetsov 2013). During the last years, numerous studies were able to show how the Hopf whole-brain model successfully simulates empirical electrophysiology (Freyer et al. 2011, 2012), MEG (Deco et al. 2017a) and fMRI (Kringelbach et al. 2015, 2023; Deco et al. 2017b; Kringelbach and Deco 2020).

The Hopf whole-brain model can be expressed mathematically as follows:

$$\frac{dx_i}{dt} = \overbrace{\left[a_i - x_i^2 - y_i^2\right]x_i - \omega_i y_i}^{Local\ Dynamics} + \overbrace{G\sum_{j=1}^{N} C_{ij}\left(x_j - x_i\right)}^{Coupling} + \overbrace{\beta\eta_i(t)}^{Gaussian\ Noise} \quad (1)$$

$$\frac{dy_i}{dt} = \left[a_i - x_i^2 - y_i^2\right]y_i + \omega_i x_i + G\sum_{j=1}^{N} C_{ij}\left(y_j - y_i\right) + \beta\eta_i(t) \quad (2)$$

Equations (1) and (2) describe the coupling of Stuart–Landau oscillators through an EC matrix C. The $x_i(t)$ term represents the simulated BOLD signal data of brain area i. The values of $y_i(t)$ are relevant to the dynamics of the system but are not part of the information read out from the system. In these equations, $\eta_i(t)$ provides additive Gaussian noise with standard deviation β. The Stuart–Landau oscillators for each brain area i express a Hopf normal form that has a supercritical bifurcation at $a_i = 0$, so that if $a_i > 0$ the system has a stable limit cycle with frequency $f_i = \omega_i/2\pi$ (where ω_i is the angular velocity); and when $a_i < 0$ the system has a stable fixed point representing a low activity noisy state. The intrinsic frequencies are fitted from the data, as given by the averaged peak frequency of the narrowband BOLD signals of each brain region. The intrinsic frequency f_i of each Stuart–Landau oscillator corresponding to a brain area i was in the 0.5–2 Hz band ($i = 1, \ldots, 360$) for the HCP MEG data used here, which was sampled at 20 ms and not further filtered. The mean power spectrum across participants from the timeseries of the MEG signal for each of the 360 cortical regions used in the analyses described here is shown in Fig. S3. The coupling term representing the input received in node i from every other node j, is weighted by the corresponding EC C_{ij}. The coupling is the canonical diffusive coupling, which approximates the simplest (linear) part of a general coupling function. G denotes the global coupling weight, scaling equally the total input received in each brain area. Although the oscillators are weakly coupled, the periodic orbit of the uncoupled oscillators is preserved.

The EC (C) matrix is derived by optimizing the conductivity of each connection in the matrix in order to fit the empirical functional connectivity ($\mathbf{FC}^{empirical}$) pairs and the lagged normalized covariance, the $\mathbf{FS}^{empirical}$ pairs. By this, we are able to infer a non-symmetric EC matrix (see Gilson et al. (2016)). We refer to this as a *generative EC model* approach because the C matrix is used to generate the functional connectivity and lagged normalized covariance matrices, and the C matrix is optimized so that the simulated matrices match the empirically measured matrices. Note that $\mathbf{FS}^{empirical}$, ie the normalized lagged covariance of the functional connectivity between pairs, lagged at τ, breaks the symmetry and thus is fundamental for our purpose. Specifically, we compute the distance between the model functional connectivity $\mathbf{FC}^{model}$ calculated analytically from the current estimate of the EC and the empirical data $\mathbf{FC}^{empirical}$, as well as the calculated model $\mathbf{FS}^{model}$ and empirical data $\mathbf{FS}^{empirical}$ and adjust each effective connection (entry in the EC matrix) separately with a gradient-descent approach. The model is run repeatedly with the updated EC until the fit converges toward a stable value.

We start with the anatomical connectivity obtained with probabilistic tractography from dMRI (or from an initial zero C_{ij} matrix) and use a pseudo gradient procedure for updating the EC matrix (see Equation 11 in the Supplementary Material). The EC matrices shown here were those computed without the structural connection matrix, as use of the structural connectivity matrix limited the connectivity to fewer links than were otherwise found with these MEG data, probably because the DTI analysis missed some connections. However, the correlation between the matrices produced with these different methods was reasonable (0.80).

Effective connectome

Whole-brain EC analysis was performed between the 25 visual cortical regions described above (see Fig. 1 and Fig. S1) and the 360 regions defined in the surface-based HCP-MMP atlas (Glasser et al. 2016) in their reordered form provided in Table S1, described in the Supplementary Material (Huang et al. 2022). This EC was computed across all 83 participants. For each participant, the mean for the 91 point long timeseries with the visual stimulus presented in bin 31 was calculated across all four trial types (faces and tools for the 0-back and 2-back trials). From this, the functional connectivity FC for the 360 cortical regions and the covariance COV of the connectivity for the 360 cortical regions calculated from the timeseries and the timeseries delayed by tau (where tau = 20 ms) was calculated for each participant, and then the FC and COV matrices were averaged across participants. These provided the inputs $\mathbf{FC}^{emp}$ and $\mathbf{COV}^{tauemp}$ to the EC algorithm ($\mathbf{COV}^{tauemp}$ refers to the $\mathbf{FS}^{empirical}$ defined above).

Functional connectivity

For comparison with the EC, the functional connectivity was also measured from the MEG signals with the identical set of participants and data. The functional connectivity was measured by the Pearson correlation between the MEG signal timeseries for each pair of brain regions, and is the $\mathbf{FC}^{emp}$ referred to above. A threshold of +0.4 is used for the presentation of the findings in Fig. 5, for this sets the sparseness of what is shown to a level commensurate with the EC, to facilitate comparison between the functional and the EC. The functional connectivity can provide evidence that may relate to interactions between brain regions, while providing no evidence about causal direction-specific effects. A high functional connectivity may in this scenario thus reflect strong physiological interactions between areas, and provides a different type of evidence to EC. The EC is non-linearly related to the functional connectivity, with effective connectivities being identified (i.e. greater than zero) only for the links with relatively high functional connectivity.

Connections shown with diffusion tractography

Diffusion tractography can provide evidence about fiber pathways linking different brain regions with a method that is completely different to the ways in which effective and functional connectivity are measured. Diffusion tractography shows only direct connections, so comparison with EC can help to suggest which effective connectivities may be mediated directly or indirectly. Diffusion tractography does not provide evidence about the direction of connections. Diffusion tractography was performed in a set of 171 HCP participants imaged at 7T with methods described in detail elsewhere (Huang et al. 2021). Some of the results are provided elsewhere (Huang et al. 2021; Rolls et al. 2023c), but

are shown in Fig. 6 for exactly the ventral visual cortical regions investigated here, to facilitate comparison.

The major parameters were: 1.05 mm isotropic voxels; a two-shell acquisition scheme with b-values = 1,000, 2,000 s/mm^2, repetition time/echo time = 7,000/71 ms, 65 unique diffusion gradient directions and 6 b0 images obtained for each phase encoding direction pair (AP and PA pairs). Pre-processing steps included distortion correction, eddy-current correction, motion correction, and gradient non-linearity correction. In brief, whole brain tractography was reconstructed for each subject in native space. To improve the tractography termination accuracy in GM, MRtrix3's 5ttgen command was used to generate multi-tissue segment images (5tt) using T1 images, the segmented tissues were then co-registered with the b0 image in diffusion space. For multi-shell data, tissue response functions in GM, WM, and CSF were estimated by the MRtrix3' dwi2response function with the Dhollander algorithm (Dhollander et al. 2016). A Multi-Shell Multi-Tissue Constrained Spherical Deconvolution model with lmax = 8 and prior co-registered 5tt image was used on the preprocessed multi-shell DWI data to obtain the fiber orientation distribution (FOD) function (Smith 2002; Jeurissen et al. 2014). Based on the voxel-wise fiber orientation distribution, anatomically-constrained tractography using the probabilistic tracking algorithm: iFOD2 (second-order integration based on FOD) with dynamic seeding was applied to generate the initial tractogram (1 million streamlines with maximum tract length = 250 mm and minimal tract length = 5 mm). To quantify the number of streamlines connecting pairs of regions, the updated version of the spherical-deconvolution informed filtering of the tractograms method was applied, which provides more biologically meaningful estimates of structural connection density (Smith et al. 2015).

Directional asymmetry of the EC

The investigation described here was performed with task-related EC. We hypothesize that use of an appropriate task may reveal the directionality of the EC in a hierarchy more fully than resting-state EC. By directional asymmetry, we mean the difference in the EC between a pair of cortical regions. In a cortical hierarchy, bottom-up or feed-forward effective connectivities are expected to be greater than top-down or feed-back effective connectivities so that input from the world rather than internal memories can dominate cortical processing (Renart et al. 1999a, 2001; Deco and Rolls 2005a, 2005b; Rolls 2023a). In the present analysis, all the cortical regions could be on one side of the brain, so this is not related to the asymmetry of the two hemispheres. For example, for the visual pathways, the directionality in the hierarchy may be revealed well by measuring the EC in the short period (e.g. 300 ms) after the visual stimulus is presented, as this is the period when the effects of the stimulus will be propagating forward up the hierarchy of visual cortical regions from V1. For comparison, with resting-state activity, signals may be propagating up and down the visual cortical hierarchy, and moreover the resting-state networks that are active may be changing, with non-visual networks sometimes active. The resting-state EC was computed from the four resting-state sessions available for the same subjects from the HCP. The timeseries for each session was approximately 14,000 long and also sampled at 50 Hz. The FC^{emp} and the COV^{tauemp} were calculated for each session, and then the average was taken over all four sessions and over all subjects to compute the resting-state EC with tau = 20 ms, as for the task-related EC, and using the same Hopf algorithm with the same parameters.

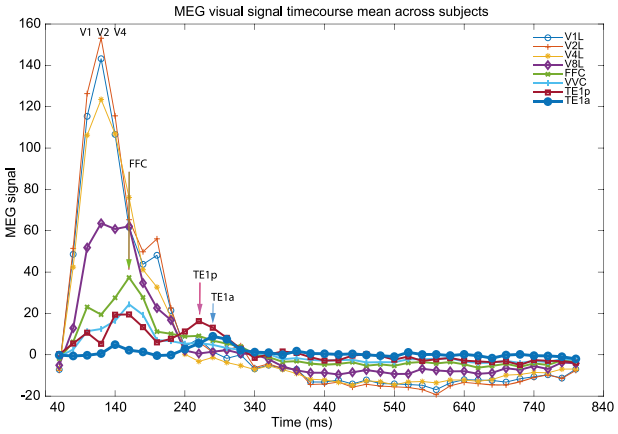

Fig. 2. The timecourse of the MEG signal in different HCP-MMP ventral visual stream cortical regions. The onset of the face or tool visual stimuli was at time 0. The amplitude of the MEG signal for the face, tool, 0-back, and 2-back conditions was averaged across 83 participants. V1, V2, and V4 are early visual cortical regions. V8 is just before the FFC. The ventral visual complex VVC probably receives from V8, is medial to the FFC (Fig. 1), is part of a route for visual information from visual cortical regions to reach the hippocampus, and is part of, or leads to, the parahippocampal scene (or place) area (Rolls et al. 2023c). TE1p is an example of an inferior temporal cortex visual region. TE1a is an example of an anterior inferior temporal cortex region involved in semantic representations (Rolls et al. 2022a, 2023c). The results are for the left hemisphere. The duration of the response may be short because fixation on the stimuli may be for only a short time period.

The measure of the directional asymmetry of the EC was the sum of the absolute differences in EC between every pair of nodes scaled by the mean of the effective connectivities across all nodes.

Results

Timecourse of ventral visual stream activity during the presentation of visual stimuli

Figure 2 shows the mean timecourse across 83 participants and across the four data sets, face, tools, 0-back, and 2-back of the amplitude MEG signal. The timeseries provided by the HCP is 91 bins long with 20 ms/bin, and the visual stimuli appeared at timebin 31. The latencies shown in Fig. 2 are with respect to timebin 31 when the visual stimuli were presented.

Figure 2 shows that V1, V2, and V4 have peaks of their response at about 120 ms, and with the 20 ms time resolution, the peaks for these three visual cortical regions are similar to each other. The relatively poor spatial resolution of MEG may also contribute to these peaks being similar.

The FFC has a peak at about 160 ms, and V8 may be intermediate between V1–V4 and the FFC.

The ventromedial visual complex VVC, which is medial to FFC (Fig. 1), has a peak at about the same time as FFC, 160 ms.

TE1p, which is in the visual inferior temporal cortex (Fig. 1), has a response with activity evident at 260 ms, and TE1a, which is more anterior in the lateral temporal lobe (Fig. 1), has a peak at about 280 ms.

These results indicate that the MEG responses for different parts of the ventral visual system do have activity with different timecourses, with greater delays with progression through the system, and thus that information is available in the MEG timeseries for EC to be calculated from these timeseries data. The results shown in Fig. 2 provide evidence about the direction of the signal transmission in the first 300 ms after visual stimulus

presentation by showing the latency and timecourse of different visual cortical regions during this time period.

Figure 2 also shows that the amplitude of the visually locked MEG time signal is greater for earlier visual cortical regions (V1, V2, V4) than for later regions (FFC, TE1p, and TE1a). This could be because almost any face or tool image will have plenty of content to activate many neurons in V1–V4, but that as representations of objects and faces are built in later cortical areas, the representations will become more sparse because of the large number of different objects and faces that must be represented (Rolls 2016, 2023a).

Overview: EC, functional connectivity, and diffusion tractography

The effective connectivities *to* the 25 ventral visual cortical regions from other cortical regions in the left hemisphere are shown in Fig. 3. Because the effective connectivities *from* the 25 visual cortical regions to other cortical regions in the left hemisphere are rather similar with the short time delay of 20 ms used for *tau* are not very different in magnitude, we show in Fig. 4 the difference of EC in the two directions. In Fig. 4, an EC that is stronger from a column to a row is shown in red, and a connectivity that is weaker from a column to a row is shown in blue (which means that blue in Fig. 4 signifies a stronger EC from a row to a column). The results in both Figs. 3 and 4 need to be considered together to interpret the EC. For comparison, the functional connectivity (measured of course with MEG) is shown in Fig. 5. For comparison, Fig. 6 shows the strength of the connections between the cortical regions measured with diffusion tractography.

V1, V2, and V4 (Group 1)

V1 and V2 have very strong EC with each other, strong with V4, and weaker with FFC, PIT, V8, VMV1–3, and VVC (Fig. 3). The EC is stronger in the direction from V1–V4 to FFC, PIT, V8, VMV1–3, and VVC and some later cortical visual regions than vice versa (Fig. 4). V4 has stronger EC to V8, PIT, and FFC than V1 and V2 (Fig. 3), which is the forward direction up the hierarchy (Fig. 4). The EC with MEG is measuring here what is expected in a hierarchical system.

The functional connectivity also shows that V1 and V2 have very strong connectivity with each other, and moderate with V4, and that V4 has stronger connectivity than V1 and V2 with FFC, PIT, and V8, but of course does not provide evidence on the directionality, as functional connectivity is measured by correlation (Fig. 5).

Usefully, the connections measured by the number of streamlines with diffusion tractography (Fig. 6) support these findings with MEG, though, again, the tractography can not address directionality.

V8, the FFC, and the PIT (Group 2)

V8, the FFC, and the PIT cortex have some EC with V1 and V2, and stronger with V4 (Fig. 3). The directionality is from V1, V2, and V4–V8, FFC, and PIT (Fig. 4), as expected in a hierarchical system and consistent with the timecourses in Fig. 2.

FFC, and to a lesser extent V8 and PIT have EC with inferior temporal cortex regions TE1p and TE2p, and with ventromedial visual regions VMV1–3 and VVC (Fig. 3). The directionality of the EC is from FFC, V8, and PIT toward the inferior temporal cortex regions TE1p and TE2p and the ventromedial visual regions (Fig. 4).

The MEG-based functional connectivity is consistent, with especially FFC having functional connectivity with the inferior temporal cortex regions TE1p and TE2p and the ventromedial visual regions (Fig. 5).

The diffusion tractography is also consistent, with FFC having connections with the inferior temporal cortex regions TE1p and TE2p and some of the ventromedial visual regions (Fig. 6).

The FFC, PIT, and V8 also receive some EC from dorsal visual division regions and MT+ visual division regions, and some parietal regions including PGi, PGs and PGp that are visual (Rolls et al. 2023c, 2023e) (Figs. 3 and 4).

The inferior temporal visual cortex TE2p and TE1p (Group 4)

The inferior temporal visual cortex TE2p and TE1p have EC with especially FFC, and also with V8 and PIT (Fig. 3), and the directionality is from FFC, V8 and PIT to inferior temporal visual cortex TE2p and TE1p (Fig. 4). The functional connectivity (Fig. 5) and the diffusion tractography (Fig. 6) also show the connectivity and connections between FFC and inferior temporal visual cortex TE2p and TE1p.

The inferior temporal cortex TE2p and TE1p then have EC (Fig. 3) directed to anterior temporal cortex regions TE1a, TE1m, TE2a, and temporal pole TGv (Fig. 4).

TE2p and TE1p have EC with a number of other cortical divisions including somatosensory (frontal opercular), auditory and STS regions, hippocampus-related medial temporal regions (Fig. 3), and in most cases, this EC is directed away from inferior temporal visual cortex regions TE2p and TE1p to these other regions (Fig. 4).

Anterior temporal lobe regions TE1a, TE1m, TE2a, TGd, and TGv (Group 5)

Inferior temporal cortex visual regions TE2p and TE1p have EC with anterior temporal lobe regions TE1a, TE1m, TE2a, and TGv (Fig. 3), and the directionality is from the inferior temporal cortex visual regions to the anterior temporal lobe regions (Fig. 4).

The anterior temporal lobe regions (and this includes TE1a, TE1m, and TE2a) have EC with a number of other cortical divisions including somatosensory (frontal opercular; Rolls et al. 2023f), auditory and superior temporal sulcus (STS) regions (Rolls et al. 2023c, 2023i), hippocampus-related medial temporal regions, orbitofrontal cortex regions (pOFC, 13l, 47m, and 47s; Rolls et al. 2023d), and Broca's area regions 44, 45, and 47l and the connected inferior frontal gyrus regions IFJa, IFJp, IFSa, IFSp (Rolls et al. 2022a) (Fig. 3), and in many of these cases this EC is directed to these anterior temporal lobe cortical areas (Fig. 4). This multimodal connectivity and other evidence implicates these anterior temporal lobe regions in semantic processing (Rolls et al. 2022a; Rolls 2023a).

The functional connectivity (Fig. 5) is generally consistent. The diffusion tractography (Fig. 6) provides evidence for direct connections between some of these anterior temporal lobe regions and the inferior temporal visual cortex TE2p and TE1p, auditory and STS regions, and medial temporal lobe regions, but do not reveal the other connectivities either because the connections are indirect, or because some of this connectivity is long-distance.

Visual inputs to medial temporal lobe regions VMV1, VMV2, VMV3, VVC, hippocampus, entorhinal cortex, perirhinal cortex, and parahippocampal gyrus TF and PHA1–3 (Group 3)

In a ventromedial visual cortical stream, regions VMV1–3 and VVC have EC with (Fig. 3) and primarily from (Fig. 4) ventral visual cortical regions the FFC, PIT, V8, TE2p, and TE1p, and also from

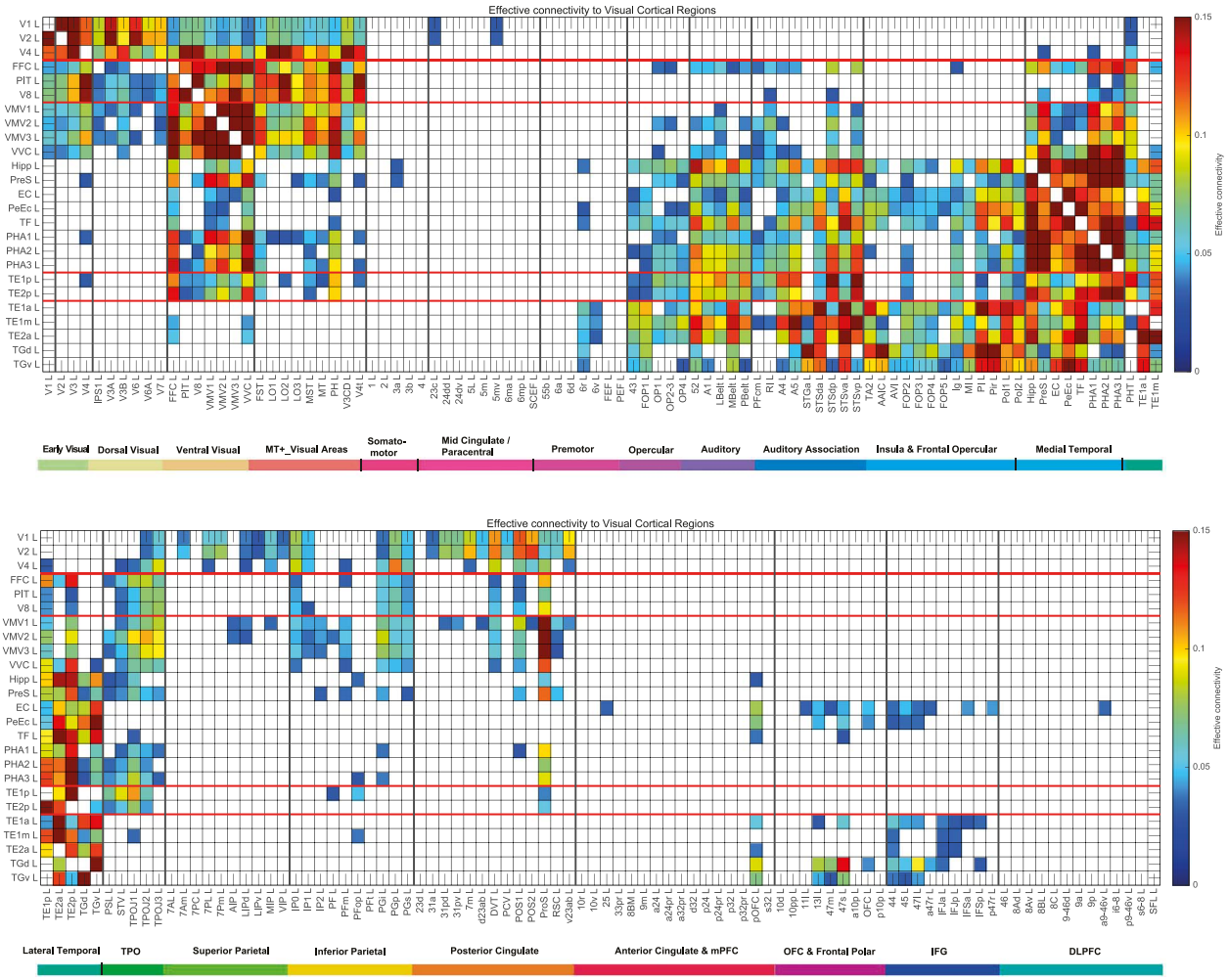

Fig. 3. EC *TO* ventral visual cortical regions (the rows) *FROM* 180 cortical areas (the columns) in the left hemisphere. The EC is read from column to row. Effective connectivities of <0.03 are shown as blank. The EC map is scaled to show 0.15 as the maximum. The EC for the first set of cortical regions is shown in the top panel; and for the second set of regions in the lower panel. Abbreviations: see Table S1. The groups of visual cortex regions are separated by red lines. Group 1 (top) early visual cortical areas V1, V2 and V4 of the HCP-MMP atlas; Group 2 intermediate cortical visual regions FFC, PIT, and V8. Group 3: medial temporal lobe visual regions with connectivity with the hippocampus. Group 4: Inferior temporal visual cortex regions TE2p and TE1p. Group 5: Multimodal anterior temporal lobe regions including the frontal pole TGd and TGv. The colored labeled bars show the cortical divisions in the HCP-MMP atlas (Glasser et al. 2016). The order of the cortical regions is that in Huang et al. (2022).

dorsal stream visual regions. The dorsal stream visual regions with high effective connectivities to VMV1–3 and VVC include FST, LO1–3, MST, MT, and V4t (Figs. 3 and 4). These VMV1–3 and VVC regions have EC with some parietal visual areas (PGI, PGp, PGs), and with some posterior cingulate division regions (including the prostriate cortex ProS and DVT which are where in humans the retrosplenial scene area is located; Sulpizio et al. 2020; Rolls et al. 2023j). VMV1–3 and VVC also have some EC from auditory association cortex regions and STS regions (Figs. 3 and 4); and have connectivity with parahippocampal (e.g. PHA1–3) and hippocampal regions (e.g. presubiculum PreS and Hipp) (Fig. 3) that tend to be directed toward these parahippocampal and hippocampal regions (Fig. 4). The parahippocampal scene area (sometimes termed the parahippocampal place area) is located where the VMV and PHA regions adjoin (Sulpizio et al. 2020; Rolls 2023c, 2023d; Rolls et al. 2023j).

In the same ventromedial visual cortical stream, a set of cortical regions in the medial part of the parahippocampal gyrus, PHA1–3, have EC with (Fig. 3), primarily from (Fig. 4), VMV1–3 and VVC regions, but also from the FFC. Many of the other effective connectivities of the medial parahippocampal gyrus PHA1–3 regions (Fig. 3) are directed away from it (Fig. 4) to the hippocampal system (perirhinal cortex PeEC, entorhinal cortex EC, and hippocampus; with other connectivities with auditory association and STS regions (Rolls et al. 2023i), and some opercular and frontal opercular somatosensory regions (Rolls et al. 2023f). This ventromedial visual pathway introduces "where" information into the human hippocampal memory system (Rolls 2023a, 2023c, 2023d; Rolls et al. 2023c).

Region TF in the lateral part of the parahippocampal gyrus has EC with (Fig. 3) primarily from (Fig. 4) lateral temporal cortical regions (TE1a, TE1m, TE1p, TE2a, TE2p, TGd, and TGv, with some from FFC). TF has strong EC with the hippocampal system (perirhinal cortex PeEC, entorhinal cortex EC, and hippocampus). TF also has some EC (Fig. 4), primarily from (Fig. 5), auditory association and STS regions (Rolls et al. 2023i) and some opercular and frontal opercular somatosensory regions (Rolls et al. 2023f). This is part of the ventrolateral visual pathway that introduces "what" information into the human hippocampal memory system (Rolls 2023a, 2023c, 2023d; Rolls et al. 2023c).

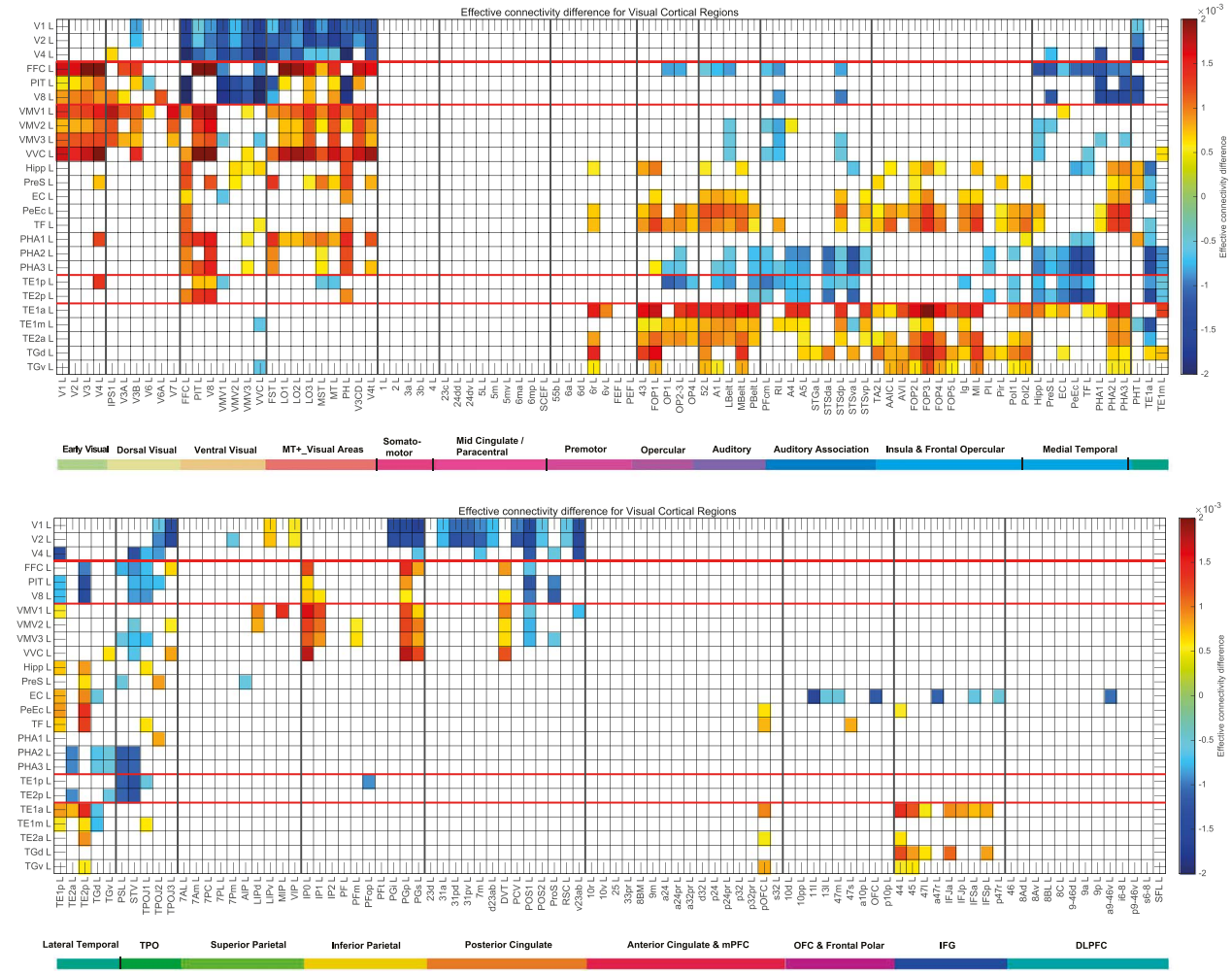

Fig. 4. Difference of the EC for ventral visual cortical regions with other cortical regions. For a given link, if the EC difference shown is positive, the connectivity is stronger in the direction from column to row. For a given link, if the EC difference shown is negative, the connectivity is weaker in the direction from column to row. The threshold value for any EC difference to be shown is 0.0005 for the connectivities shown in Fig. 3. The abbreviations for the brain regions are shown in Table S1, and the brain regions are shown in Fig. 1 and Fig. S1. The EC difference for the first set of cortical regions is shown in the top panel; and for the second set of regions in the lower panel. Conventions as in Fig. 3.

Directional asymmetry of the EC

The task-related EC network for the 25 ventral visual stream regions analyzed here had more directional asymmetry than the resting state-related EC, with the mean for the task-related asymmetry 0.0042, and for the resting state 0.0003 (paired $t = 30.1$, $df = 624$, $P < 10^{-122}$) (Fig. S2). (The measure of the directional asymmetry of the EC was the sum of the absolute differences in EC between every pair of nodes scaled by the mean of the effective connectivities across all nodes.) This was as predicted (see Methods). An implication is that use of the task-related EC (as used here) may, at least with MEG data, reveal the directional asymmetry in the effective connectivities better than the resting-state EC.

Discussion

The analysis of the EC with MEG of the ventral visual streams described here provides important evidence on the hierarchical organization of the system, because MEG with its fast data acquisition (in the order of ms) can be used to follow visual processing through the system in response to visual stimuli delivered during task performance. V1, V2, V3, and V4 formed a first Group of interconnected regions. A second Group consisted of V8, the FFC, and the PIT cortex, which had stronger connectivity from V4 than V1 and V2. In a ventrolateral stream, inferior temporal cortex regions TE2p and TE1p received from the FFC, V8 and PIT and also ventromedial VMV regions. Group 5 in the anterior temporal lobe consisting of TE1a, TE1m, TE2a, and also TGv receive EC from TE2p and TE1p, but are multimodal in that they receive also from STS visual–auditory regions, from somatosensory, auditory, orbitofrontal cortex, Broca's regions 44 and 45 and related inferior frontal gyrus regions. In a ventromedial visual stream (Group 3), VMV1–3 and VVC receive from V1 to V4 but also from FFC, V8, TE2p, and TE1p and from dorsal stream (especially MT+) visual regions. In the same ventromedial stream, the medial parahippocampal gyrus PHA1–3 receive from the VMV regions (which together include the parahippocampal scene area) but also from FFC, and have connectivity to the hippocampal system regions the perirhinal cortex, entorhinal cortex, and hippocampus.

The analysis of generative EC in this hierarchically organized system (Figs. 3 and 4) is supported by the timecourses of the responses of different visual cortical regions shown in Fig. 2.

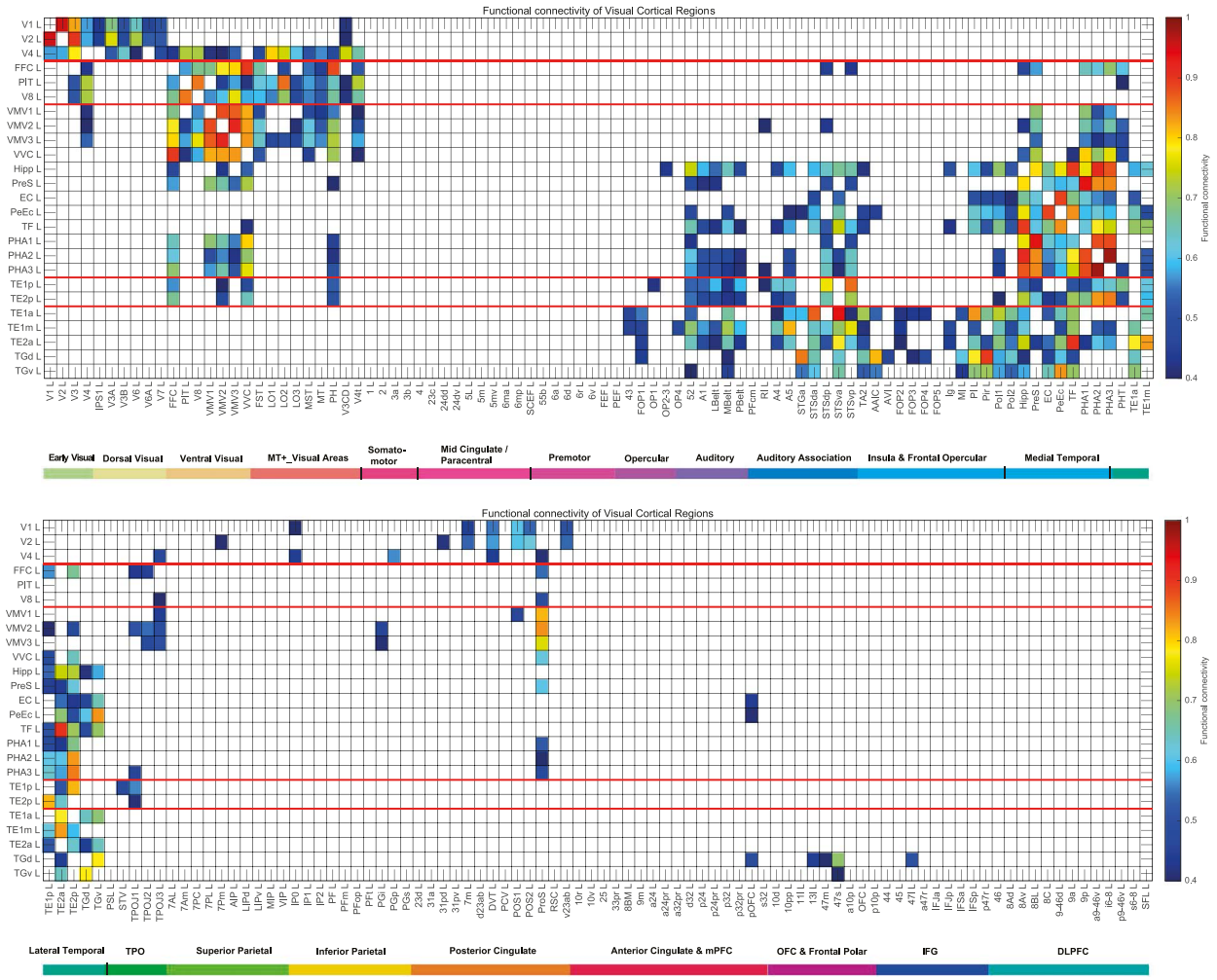

Fig. 5. Functional connectivity between ventral visual cortical regions and 180 other cortical regions in the left hemisphere. Functional connectivities less than 0.4 are shown as blank. The upper figure shows the functional connectivity of the visual cortical regions with the first half of the cortical regions; the lower figure shows the functional connectivity with the second half of the cortical regions. Abbreviations: see Table S1. Conventions as in Fig. 3. An unthresholded version of this figure is provided for completeness in Fig. S4.

Some key features of the EC of the ventral visual pathways measured with MEG (Figs. 3 and 4, with schematic summaries in Figs. 7 and 8) are highlighted next, and compared with the results obtained with fMRI (see Figs. 1 and 3 of Rolls et al. 2023c). Points taken into consideration in this comparison are that with fMRI, the spatial resolution is better than with MEG; and that the differences between the ECs in the two directions are smaller with MEG, perhaps related to the small value of tau = 20 ms used to establish the directionality with MEG; and that the MEG is acquired during a visual task, whereas the fMRI is resting state. Discussion of some of the functions of the cortical regions analyzed here are provided elsewhere (Rolls 2023a; Rolls et al. 2023c).

First, V1–V4 have relatively high EC with each other with both MEG and fMRI. Second, FFC, PIT, and V8 receive forward EC from especially V4 and to some extent from earlier regions V2, V3, and V1 with both MEG and fMRI.

Third, FFC has EC directed to TE1p with fMRI, and this is shown more clearly with MEG from FFC, PIT and V8 to TE1p and TE2p. FFC, PIT, and V8 also have EC directed to medial parahippocampal VMV1–3 and VVC with both MEG and fMRI.

Fourth, MEG shows more clearly the hierarchical nature of the EC from TE1p and TE2p to the more anterior temporal lobe regions TE1a, TE1m, and TE2a, and also to lateral parahippocampal TF, than fMRI. MEG also shows more clearly that TE1p and TE2p have connectivity directed toward STS regions (STSda, STSdp, STSva, STSvp), and that these STS regions have, in turn, EC directed to anterior temporal lobe regions TE1a, TE1m, TE2a, and TGd (Fig. 4).

Thus overall the findings from EC with MEG are consistent with those with fMRI, with factors that are likely to contribute to the differences the poorer spatial resolution of MEG, and the visual task being performed during the MEG data acquisition. In a preliminary analysis with resting-state MEG from the same HCP participants, we have found that although the EC differences in the two directions are smaller than during the visual task (Fig. S2), a similar overall hierarchy is evident.

These effective connectivities measured with MEG are helpful in supporting effective connectivities measured in the same systems with fMRI. The fMRI investigation (Rolls et al. 2023c) with which the present MEG investigation can be compared, because the HCP-MMP atlas is used in both and because many of the HCP participants are the same, have a much slower data acquisition rate (1 s) with tau set to 2 s as this is the fastest time within which a change in the fMRI signal due to an input from another brain region might be expected to be detected. For comparison, for the MEG investigation described here, tau was 20 ms. Another difference was that resting-state data were analyzed in

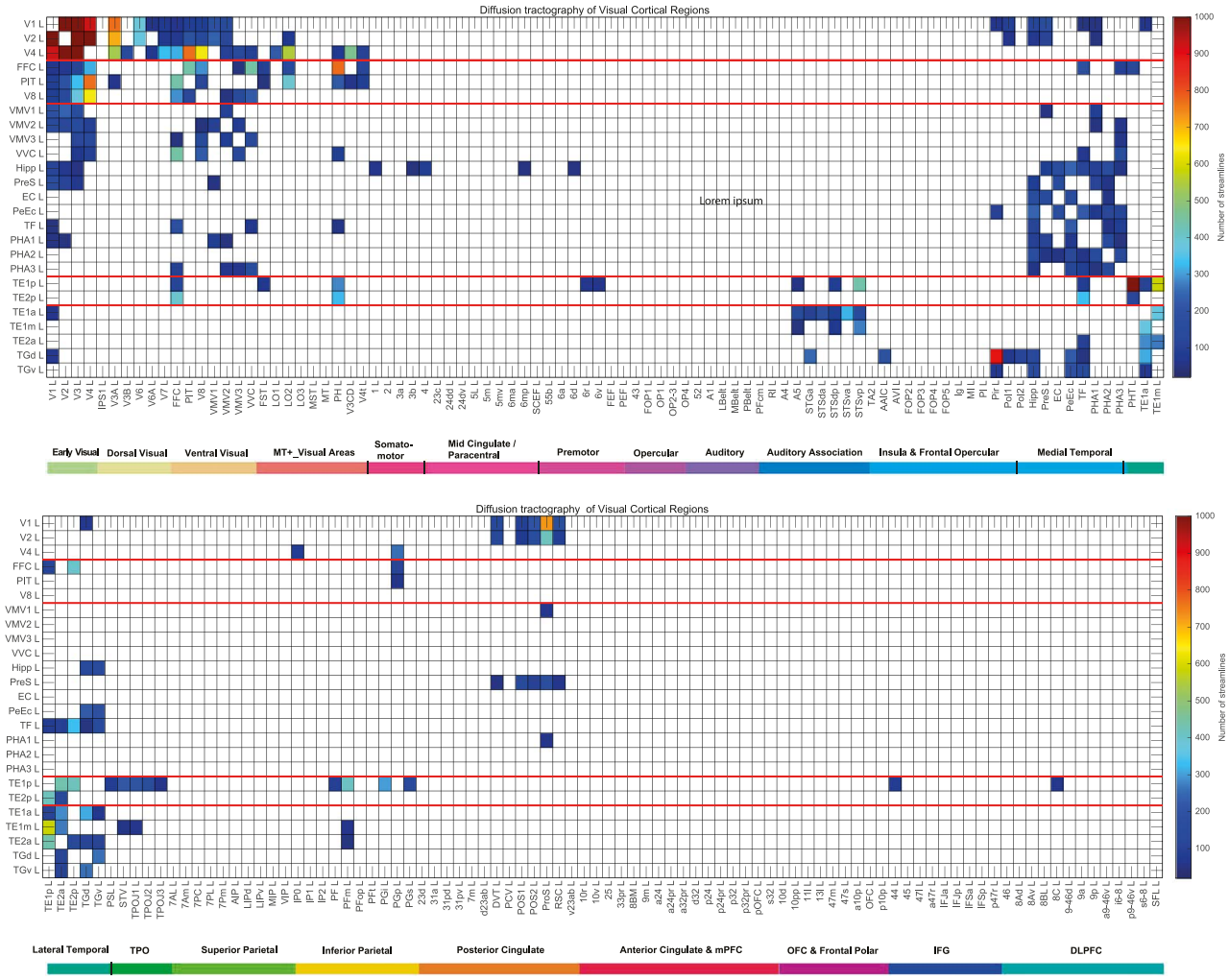

Fig. 6. Connections between the ventral visual cortical regions and 180 other cortical regions in the left hemisphere as shown by diffusion tractography using the same layout as in Figs. 3–5. The number of streamlines shown was thresholded at 50 and values less than this are shown as blank. The color bar was threshold at 1,000 streamlines (see the text). Abbreviations: see Table S1. Conventions as in Fig. 3.

the fMRI investigation (Rolls et al. 2023c). The hierarchical organization reported with the fMRI investigation (Figs. 6 and 7 of Rolls et al. 2023c) fits the hierarchical organization described here with MEG, although the MEG may not allow such good discrimination between each individual step in the hierarchies, perhaps because of its poorer spatial resolution. We base the directionality in the hierarchy described here on task-related MEG, and note that the directionality measured with fMRI may appear to be different for at least two reasons. One is that with fMRI the data analyzed (Rolls et al. 2022b, 2023b, 2023c, 2023d, 2023e, 2023f, 2023I, 2023j) were for the resting state, and were not task-related, with task-related expected to show the directionality better. Indeed, we have found with the MEG analyses that the directional asymmetry is greater between the forwards and backwards directions with task-related data than with resting-state data (Fig. S2); and that using a long tau in the MEG resting-state analysis, of e.g. 1,000 ms, can have an influence on the measured directionality. The second is that the MEG analysis is on a fast timescale, with tau = 20 ms, whereas with fMRI, the tau is 2,000 ms, which may allow slow top-down effects to contribute to the measured directionality using resting-state fMRI. For example, after visual input reaches the anterior temporal lobe in approximately 280 ms (Fig. 2), there may be continuing activity supported, for example, by the connectivity with the prefrontal cortex, and that continuing activity could be a source of top-down effects on earlier regions in the hierarchy that may be evident with long time delays of e.g. 2,000 ms used for tau in the fMRI. The directionality reported in the resting-state fMRI papers (Rolls et al. 2022b, 2023b, 2023c, 2023d, 2023e, 2023f, 2023i, 2023j) is consistent with that reported here using task-related MEG, namely that signal propagation should be forwards from early visual cortical areas such as V1–V4 to higher cortical visual areas such as FFC, V8, PIT, and then to TE1p and TE2p, and then to anterior temporal lobe regions such as TE1a and TE1m. Indeed, the visual signal is expected to propagate through visual cortical areas in a hierarchy with about 15–20 ms per stage (Wallis and Rolls 1997; Panzeri et al. 2001; Rolls 2016, 2023a), which is supported by the MEG data shown in Fig. 2 if extra time is allowed for the greater distance between cortical regions in the human brain (Rolls 2023a).

The utility of the EC measured with MEG in validating the effective connectivities measured with rs-fMRI (Rolls et al. 2022a, 2022b, 2023b, 2023c, 2023d, 2023e, 2023f, 2023i, 2023j) is supported by the following further points. For the task-related MEG data analyzed here, hierarchical organization was also evident in the somatosensory system from somatosensory regions 3a, 3b, 1, and 2 to opercular regions (OP) to frontal opercular regions (FOP) to

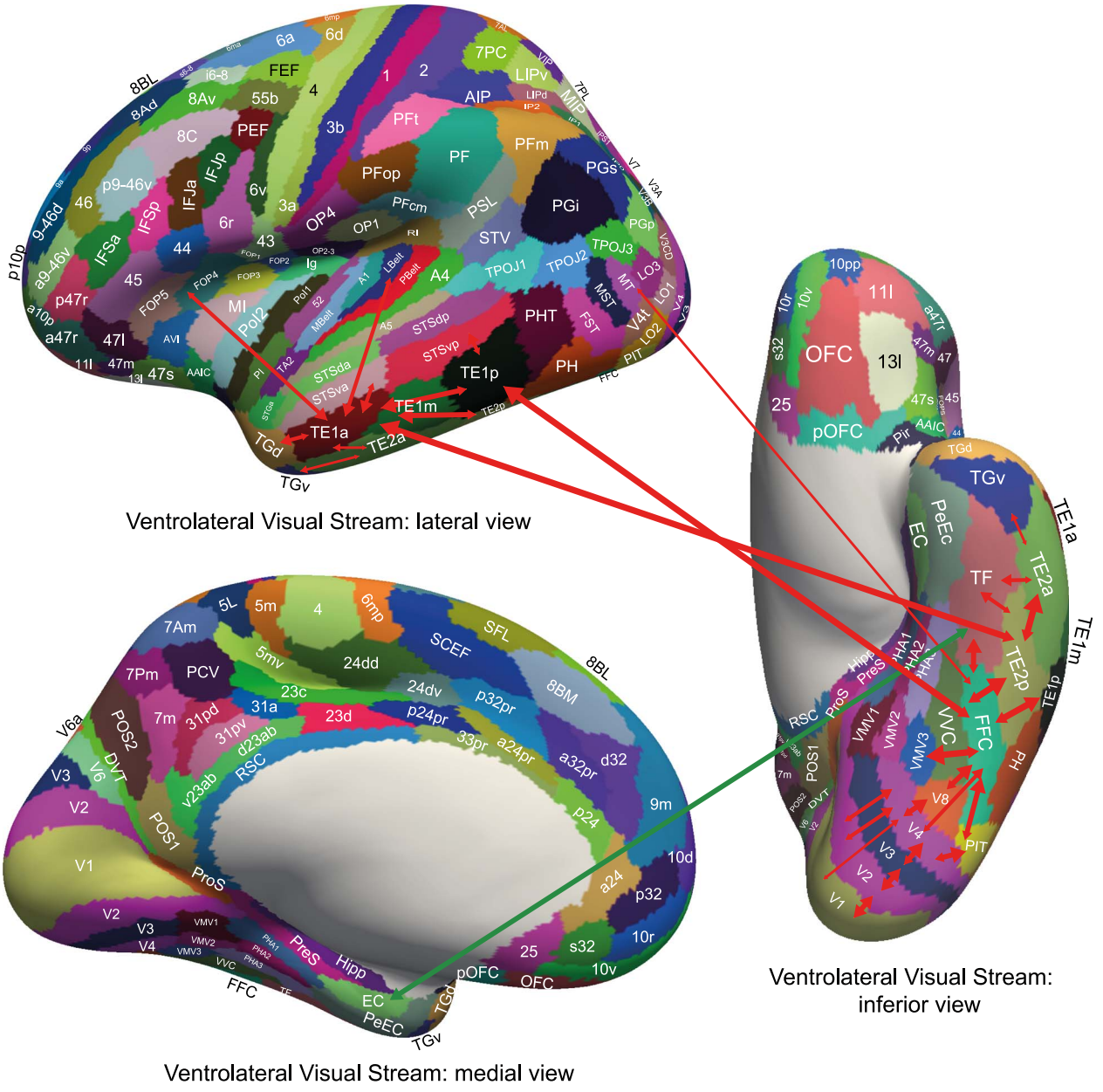

Fig. 7. Hierarchical organization of the ventrolateral visual cortical stream measured with MEG EC: schematic overview based on the results shown in Figs. 3 and 4. In the first level, V1, V2, and V3 connect with V4. In the second level, especially V4 has connectivity to FFC, V8, and PIT. In the third level, FFC, V8, and PIT have connectivity to TE1p and TE2p, which are the last mainly unimodal visual inferior temporal cortex regions where faces and objects are represented. In the fourth level, TE1p and TE2p have connectivity to TE1m, TE2a, TE1a, and the temporal pole TGd and TGd. This fourth level anterior temporal lobe region is multimodal, in that it also receives auditory cortex input from auditory cortex regions such as the Belt regions; and from somatosensory regions in the frontal operculum (FOP) and opercular (OP) regions. A green arrow shows how the ventrolateral visual stream provides "what" input to the hippocampal memory system via parahippocampal gyrus TF to perirhinal PeEc, hippocampus, etc. The widths of the lines and the size of the arrowheads indicate the magnitude and direction of the EC.

the insula (cf. Rolls et al. 2023f). Hierarchical organization was also evident in the auditory system from early auditory cortical regions (A1) and Belt regions to A5, TA2 and the auditory regions in the STS, and then on to regions that include the temporal pole, orbitofrontal cortex, Broca's region 44, and the related inferior frontal gyrus (cf. Rolls et al. 2023i).

As shown in the results and in Fig. S2, the directional asymmetry of the EC in the visual pathways was greater for the visual task than for the resting state. We relate this to the following. For the visual pathways, the directionality in the hierarchy may be revealed well by measuring the EC in the short period (e.g. 300 ms) after the visual stimulus is presented, as this is the period when the effects of the stimulus will be propagating forward up the hierarchy of visual cortical regions from V1 (Fig. 2). In comparison, with resting-state activity, signals may be propagating up and down the visual cortical hierarchy over long periods without visual stimuli being shown, and moreover the resting-state networks that are active may be changing, with non-visual networks sometimes active. An implication is that use of the task-related EC (as used here) may, at least with MEG data, reveal the directional asymmetry in the effective connectivities better than the resting state.

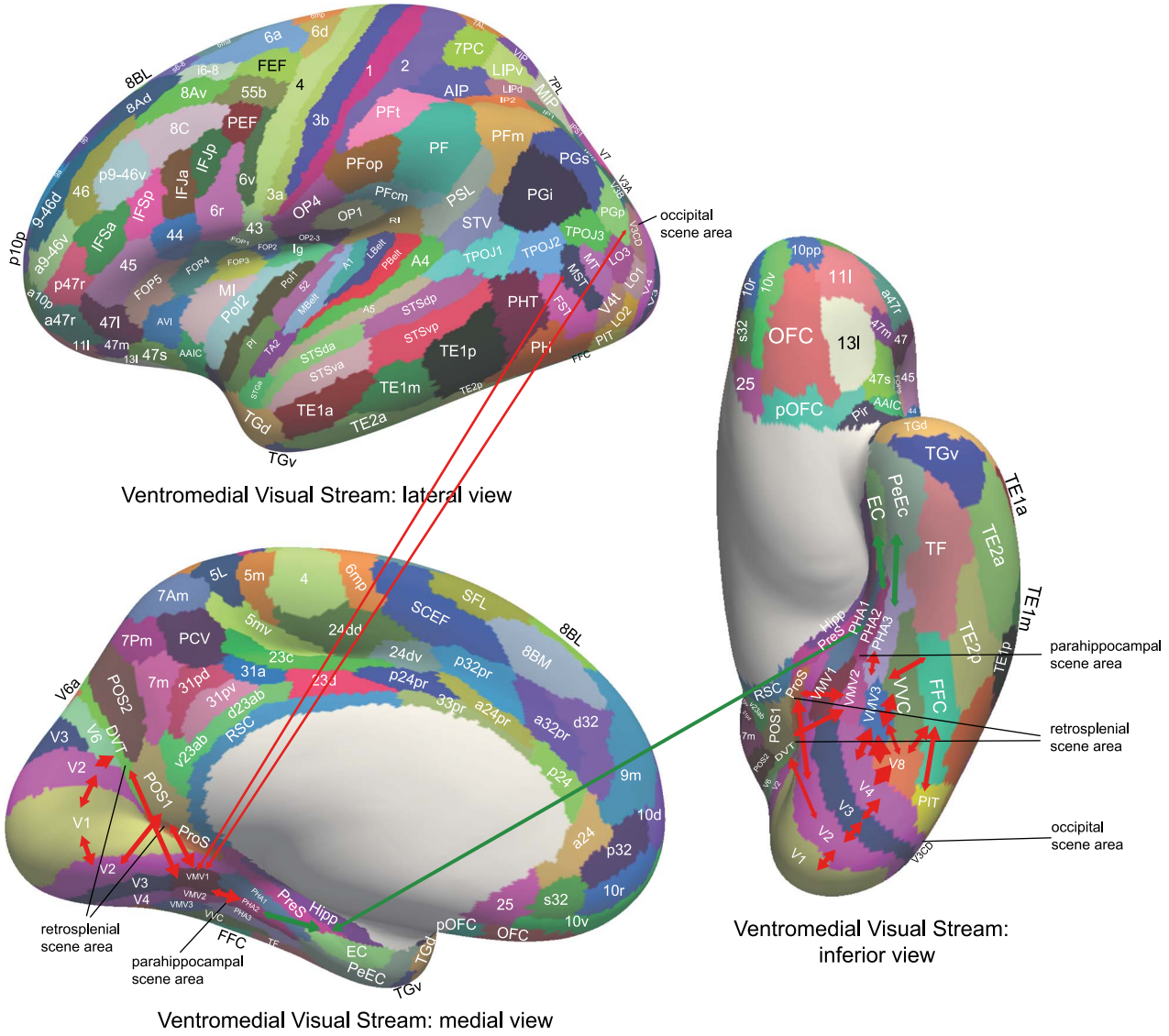

Fig. 8. Hierarchical organization of the ventromedial visual cortical stream measured with MEG EC: schematic overview. In the first level, after V1, V2 has connectivity to DVT (the dorsal transitional visual area) and ProS (the prostriate cortex) that are where the retrosplenial scene area is located in humans. In the second level, DVT and ProS have connectivity to ventromedial visual regions (VMV1–3 and VVC). These ventromedial visual regions also have EC from V3CD where the occipital scene area is located, from the nearby inferior parietal PGp region, and from MT, MST, etc. in the dorsal visual stream. In the third level, the ventromedial visual regions have EC to the medial parahippocampal regions PHA1–3. The medial parahippocampal regions PHA1–3 also have EC from the ventrolateral stream region FFC (and also from some STS and auditory regions). The parahippocampal scene area is located at the intersection of the ventromedial visual regions (VMV1–3 and VVC) and medial parahippocampal regions PHA1–3. In the fourth level, the medial parahippocampal regions PHA1–3 have connectivity to the hippocampal memory system (green arrow). The widths of the lines and the size of the arrowheads indicate the magnitude and direction of the EC.

The difference of the effective connectivities in the two directions between every pair of nodes is an interesting parameter, and it is not clear how accurately the current Hopf algorithm and data allow this to be measured. For reasons related to how different networks in the brain interact, the coupling should not be too strong, or the two separate brain regions will be too strongly locked together and will not be able to compute something different (Renart et al. 1999a; Rolls 2016, 2023a). The regime in which two coupled attractor networks can operate to some extent independently, but where one can act as a trigger to another, or where the networks interact usefully as in top-down attention, is where the coupling g between the two attractor networks is in the order of $g = 0.1$, indicating that the strength of the interconnectivity should be about 0.1 of the connectivity within each attractor network (Renart et al. 1999a, 1999b; Rolls et al. 2012; Rolls and Deco 2015; Rolls 2023a). But the effects of different ratios for the connectivity in the two directions has been less explored (Rolls et al. 2012; Rolls and Deco 2015; Rolls 2023a). One additional point is of interest: whatever the forward and backward effective connectivities may be between two brain regions in a hierarchy in the cerebral cortex, the representation at a higher level is not transferred back to early levels. For example, neurons in V1 do not have large receptive fields of 70° with selective tuning to different objects or faces, yet this is what is represented in the inferior temporal visual cortex (Rolls 2016, 2023a). The functions of the cortico-cortical backprojections/top down influences therefore have different functions than transferring representations back down the hierarchy, and these functions include top-down attention and memory recall (Rolls 2016, 2023a). For these functions to operate correctly, and in such a way that

the top-down modulation does not dominate bottom-up input from the world, the backprojections need to be weaker than the feedforward bottom-up connections, as analyzed and described elsewhere (Renart et al. 1999a, 1999b; Deco and Rolls 2005a, 2005b; Rolls 2016, 2018; Rolls et al. 2023a, 2023d, 2023c).

It is interesting that the latency of the peak of the MEG response is quite long in regions such as posterior inferior temporal visual cortex (TE1p 260 ms) and anterior temporal lobe (semantic) cortex (TE1a 280 ms, see Fig. 2). Part of this is related to the peak of the MEG response in V1, V2, and V4, which is 100 ms, with some response evident at 60 ms. In macaques, the time for the operation of each cortical stage of visual processing is approximately 15 ms (Rolls 1992, 2023a), even allowing for the recurrent dynamical processing within each cortical region (Panzeri et al. 2001; Rolls 2023a). The longer latencies in humans may be related to the longer transmission distances, and also perhaps for recurrent processing between many cortical regions that are required to build semantic representations in human anterior temporal cortex TE regions (Rolls et al. 2022a, 2023c; Rolls 2023a). In any case, the faster transmission times likely in dorsal stream visual cortical regions did not contribute to the present results, which focused on ventral stream visual cortical regions.

In a previous MEG investigation, the feedforward Granger causality was greater in most cases then the feedback Granger causality in the gamma band (40–75 Hz), with the reverse in the alpha-beta band (7–19 Hz) (Michalareas et al. 2016). However, that investigation is not closely comparable to the present investigation in that forward vs backward directionality was measured not by the known position anatomically and by neurophysiological analysis in the hierarchy, but instead by analysis of feedforward vs feedback anatomical connections between any pair of cortical regions in macaques, and the cortical regions included regions in both the dorsal and ventral visual streams that may have different processing speeds. It is also noted that that investigation did not investigate the VMV and PHA regions leading toward the hippocampal memory system, and that this is a key pathway analyzed in the present investigation.

The new findings made possible by this MEG design include the following. (i) The signal flow through ventral stream visual cortical regions in the first 300 ms after visual stimulus presentation from V1, V2, and V4 to V8, and then the FFC, and then posterior inferior temporal cortex TE1p, and then anterior temporal lobe regions such as TE1a has been made clear (Fig. 2) in a way that is not possible with fMRI. (ii) The MEG analysis of EC and functional connectivity and connections measured with DTI of ventral stream visual cortical regions including VMV and PHA regions is performed for the first time using the HCP-MMP parcellation of the cerebral cortex, which not only is the best defined parcellation of the cerebral cortex as it uses anatomical, functional connectivity, and task-related fMRI activation data to define 360 cortical regions (Glasser et al. 2016), but also allows direct comparison with HCP fMRI data analyzed using the same atlas (Rolls et al. 2022a, 2023c). (iii) The analysis here shows, based on the latency of activation of visual cortical regions (Fig. 2), and the consistent directionality of the EC shown in Fig. 5, that with the fast neuroimaging method of MEG it is possible to measure the forward signal flow and the corresponding forward-directed EC up through cortical hierarchies, the lateral and medial ventral visual cortical streams. This is important, for the EC when measured with the BOLD fMRI time signal, which is much slower with a time to respond taken as tau = 2 s, appears to show EC in the reverse direction, though the sign was set in our previous papers to show what should be the correct forward connectivity up through the visual system (Rolls et al. 2023c) that is now confirmed with MEG. An independent fMRI investigation has confirmed this by showing, using the Gilson et al. EC algorithm (Gilson et al. 2016), that the EC measured with the BOLD signal is stronger from V3 to V2, and from V2 to V1, than vice versa (Gravel et al. 2020). Possible reasons for the reverse effect measured with the BOLD signal such as top-down effects of reverberating neural activity in higher including short-term memory cortical regions that dominate the processing over the long time period of 2 s have been considered above. It is noted that in our papers involving the measurement of EC (Rolls et al. 2022a, 2022b, 2023b, 2023c, 2023d, 2023e, 2023f, 2023i, 2023j), the connectivity has always been shown with the required sign reversal for the BOLD signal measurement to show the stronger EC in the bottom-up forward direction that is based on evidence from neurophysiology and from anatomical connections (Kandel et al. 2021; Rolls 2023a).

In addition, it is important that the analysis described here with MEG measures EC in the period 1.2 s after visual stimulus presentation (the visual stimuli are presented at bin 31 in the time series of 91 time bins with sampling every 20 ms), so the results with MEG measure mainly the effects from V1 up through visual cortical regions given the time courses shown in Fig. 2, which support the EC directionalities shown in Fig. 4. It is also important that the effective connectivities measured with MEG for the ventral stream cortical regions are generally consistent with those measured with the BOLD fMRI signal (Rolls et al. 2023c) apart from the directionality, and the lower spatial resolution of MEG. It is also the case that the difference in the magnitude of the directionality measured with MEG is small (Fig. 4), which is probably because tau = 20 ms is a short time period.

In conclusion, the effective connectivities of two ventral visual cortical streams measured with task-related MEG provide complementary support to the hierarchical organization of brain systems measured with resting-state fMRI (Rolls et al. 2022a, 2022b, 2023b, 2023c, 2023d, 2023e, 2023f, 2023I, 2023j), and help to reveal the hierarchical organization of the visual cortical regions in humans. We show for example two visual pathways to the hippocampal episodic memory system in humans. One is a ventromedial visual pathway from V1 to V4 via VMV and medial hippocampal regions PHA1–3 where the parahippocampal scene or place area is located to provide scene ("where") information to the hippocampal episodic memory system. The second is a ventrolateral visual stream from V1 to V4 via V8, FFC and PIT to PIT cortex TE1p and TE2p and then to the lateral parahippocampal region TF to provide "what" information about faces and objects to the hippocampal episodic memory system. Understanding these pathways to the hippocampal episodic memory system is leading to a deep re-evaluation of the types of "where" and "what" inputs that are fundamental for understanding the functions of the human and non-human primate hippocampal system in episodic memory (Rolls et al. 2023a, 2023c, 2023d). It is also revealed with MEG how the ventrolateral visual pathways reach the human anterior temporal lobe which is shown to be multimodal and therefore suited to building semantic representations (Rolls et al. 2022a; Rolls 2023a). The use of the fast neuroimaging modality MEG in this investigation helps to reveal the directionality of these effective connectivities when visual stimuli are being presented in a task.

Acknowledgments

The neuroimaging data were provided by the Human Connectome Project, WU-Minn Consortium (Principal Investigators: David Van

Essen and Kamil Ugurbil; 1U54MH091657) funded by the 16 NIH Institutes and Centers that support the NIH Blueprint for Neuroscience Research; and by the McDonnell Center for Systems Neuroscience at Washington University.

Supplementary Material

Supplementary material is available at Cerebral Cortex Journal online.

Author contributions

Edmund Rolls designed and performed the research, and wrote the paper. Gustavo Deco provided the generative effective connectivity algorithm. Yi Zhang converted the HCP MEG data into the HCP-MMP1 surface parcellation. J.Feng performed the funding acquisition. All authors approved the paper.

Funding

The work was supported by the following grants. Professor JF: National Key R&D Program of China (No. 2019YFA0709502); 111 Project (No. B18015); Shanghai Municipal Science and Technology Major Project (No. 2018SHZDZX01), ZJLab, and Shanghai Center for Brain Science and Brain-Inspired Technology; and National Key R&D Program of China (No. 2018YFC1312904). GD is supported by a Spanish National Research Project (ref. PID2019-105772GB-I00 MCIU AEI) funded by the Spanish Ministry of Science, Innovation and Universities (MCIU), State Research Agency (AEI); HBP SGA3 Human Brain Project Specific Grant Agreement 3 (grant agreement no. 945539), funded by the EU H2020 FET Flagship programme; SGR Research Support Group support (ref. 2017 SGR 1545), funded by the Catalan Agency for Management of University and Research Grants (AGAUR); Neurotwin Digital twins for model-driven non-invasive electrical brain stimulation (grant agreement ID: 101017716) funded by the EU H2020 FET Proactive programme; euSNN European School of Network Neuroscience (grant agreement ID: 860563) funded by the EU H2020 MSCA-ITN Innovative Training Networks; CECH The Emerging Human Brain Cluster (Id. 001-P-001682) within the framework of the European Research Development Fund Operational Program of Catalonia 2014–2020; Brain-Connects: Brain Connectivity during Stroke Recovery and Rehabilitation (id. 201725.33) funded by the Fundacio La Marato TV3; Corticity, FLAG¨ERA JTC 2017 (ref. PCI2018-092891) funded by the Spanish Ministry of Science, Innovation and Universities (MCIU), State Research Agency (AEI). The funding sources had no role in the study design; in the collection, analysis, and interpretation of data; in the writing of the report; and in the decision to submit the article for publication.

Conflict of interest statement: None declared.

CRediT author statement

Edmund Rolls (Conceptualization, Data curation, Formal analysis, Investigation, Methodology, Project administration, Resources, Software, Supervision, Validation, Visualization, Writing—original draft, Writing—review and editing), Gustavo Deco (Conceptualization, Formal analysis, Software, Writing—review and editing), Yi Zhang (Data curation, Writing—review and editing), and Jianfeng Feng (Project administration, Resources).

Ethical permissions

No data were collected as part of the research described here. The data were from the Human Connectome Project, and the WU-Minn HCP Consortium obtained full informed consent from all participants, and research procedures and ethical guidelines were followed in accordance with the Institutional Review Boards (IRB), with details at the HCP website http://www.humanconnectome.org/

Data and code availability

The data are available at the HCP website http://www.humanconnectome.org/. Basic code for the Hopf generative effective connectivity algorithm is available at https://github.com/decolab/gec.

References

Bajaj S, Adhikari BM, Friston KJ, Dhamala M. Bridging the gap: dynamic causal modeling and Granger causality analysis of resting state functional magnetic resonance imaging. *Brain Connect*. 2016:6:652–661.

Baker CM, Burks JD, Briggs RG, Conner AK, Glenn CA, Taylor KN, Sali G, McCoy TM, Battiste JD, O'Donoghue DL, et al. A Connectomic atlas of the human cerebrum-Chapter 7: the lateral parietal lobe. *Oper Neurosurg (Hagerstown)*. 2018:15:S295–S349.

Baker CM, Burks JD, Briggs RG, Milton CK, Conner AK, Glenn CA, Sali G, McCoy TM, Battiste JD, O'Donoghue DL, et al. A Connectomic atlas of the human cerebrum-Chapter 6: the temporal lobe. *Oper Neurosurg (Hagerstown)*. 2018:15:S245–S294.

Baxter MG, Murray EA. Effects of hippocampal lesions on delayed nonmatching-to-sample in monkeys: a reply to Zola and Squire (2001). *Hippocampus*. 2001a:11:201–203.

Baxter MG, Murray EA. Opposite relationship of hippocampal and rhinal cortex damage to delayed nonmatching-to-sample deficits in monkeys. *Hippocampus*. 2001b:11:61–71.

Buckley MJ, Gaffan D. Perirhinal cortical contributions to object perception. *Trends Cogn Sci*. 2006:10:100–107.

Colclough GL, Smith SM, Nichols TE, Winkler AM, Sotiropoulos SN, Glasser MF, Van Essen DC, Woolrich MW. The heritability of multi-modal connectivity in human brain activity. *Elife*. 2017:6:e20178.

Deco G, Rolls ET. Attention, short-term memory, and action selection: a unifying theory. *Prog Neurobiol*. 2005a:76:236–256.

Deco G, Rolls ET. Neurodynamics of biased competition and cooperation for attention: a model with spiking neurons. *J Neurophysiol*. 2005b:94:295–313.

Deco G, Cabral J, Woolrich MW, Stevner ABA, van Hartevelt TJ, Kringelbach ML. Single or multiple frequency generators in on-going brain activity: a mechanistic whole-brain model of empirical MEG data. *NeuroImage*. 2017:152:538–550.

Deco G, Kringelbach ML, Jirsa VK, Ritter P. The dynamics of resting fluctuations in the brain: metastability and its dynamical cortical core. *Sci Rep*. 2017:7:3095.

Deco G, Cruzat J, Cabral J, Tagliazucchi E, Laufs H, Logothetis NK, Kringelbach ML. Awakening: predicting external stimulation to force transitions between different brain states. *Proc Natl Acad Sci*. 2019:116:18088–18097.

Dhollander T, Raffelt D, Connelly A. *Unsupervised 3-tissue response function estimation from single-shell or multi-shell diffusion MR data without a co-registered T1 image. ISMRM workshop on breaking the barriers of diffusion MRI* 5; 2016.

Frassle S, Lomakina EI, Razi A, Friston KJ, Buhmann JM, Stephan KE. Regression DCM for fMRI. *NeuroImage*. 2017:155: 406–421.

Freyer F, Roberts JA, Becker R, Robinson PA, Ritter P, Breakspear M. Biophysical mechanisms of multistability in resting-state cortical rhythms. *J Neurosci*. 2011:31:6353–6361.

Freyer F, Roberts JA, Ritter P, Breakspear M. A canonical model of multistability and scale-invariance in biological systems. *PLoS Comput Biol*. 2012:8:e1002634.

Friston K. Causal modelling and brain connectivity in functional magnetic resonance imaging. *PLoS Biol*. 2009:7:e33.

Gilson M, Moreno-Bote R, Ponce-Alvarez A, Ritter P, Deco G. Estimation of directed effective connectivity from fMRI functional connectivity hints at asymmetries in the cortical connectome. *PLoS Comput Biol*. 2016:12:e1004762.

Glasser MF, Coalson TS, Robinson EC, Hacker CD, Harwell J, Yacoub E, Ugurbil K, Andersson J, Beckmann CF, Jenkinson M, et al. A multimodal parcellation of human cerebral cortex. *Nature*. 2016:536: 171–178.

Gravel N, Renken RJ, Harvey BM, Deco G, Cornelissen FW, Gilson M. Propagation of BOLD activity reveals task-dependent directed interactions across human visual cortex. *Cereb Cortex*. 2020:30: 5899–5914.

Huang C-C, Rolls ET, Hsu C-CH, Feng J, Lin C-P. Extensive cortical connectivity of the human hippocampal memory system: beyond the "what" and "where" dual-stream model. *Cereb Cortex*. 2021:31: 4652–4669.

Huang CC, Rolls ET, Feng J, Lin CP. An extended Human Connectome Project multimodal parcellation atlas of the human cortex and subcortical areas. *Brain Struct Funct*. 2022:227: 763–778.

Jeurissen B, Tournier JD, Dhollander T, Connelly A, Sijbers J. Multitissue constrained spherical deconvolution for improved analysis of multi-shell diffusion MRI data. *NeuroImage*. 2014:103: 411–426.

Kandel ER, Koester JD, Mack SH, Siegelbaum SA, editors. *Principles of neural science*. 6th ed ed. City. New York: McGraw-Hill; 2021.

Kringelbach ML, Deco G. Brain states and transitions: insights from computational neuroscience. *Cell Rep*. 2020:32:108128.

Kringelbach ML, McIntosh AR, Ritter P, Jirsa VK, Deco G. The rediscovery of slowness: exploring the timing of cognition. *Trends Cogn Sci*. 2015:19:616–628.

Kringelbach ML, Perl YS, Tagliazucchi E, Deco G. Toward naturalistic neuroscience: mechanisms underlying the flattening of brain hierarchy in movie-watching compared to rest and task. *Sci Adv*. 2023:9:eade6049.

Kuznetsov YA. *Elements of applied bifurcation theory*. New York: Springer Science and Business Media; 2013.

Larson-Prior LJ, Oostenveld R, Della Penna S, Michalareas G, Prior F, Babajani-Feremi A, Schoffelen JM, Marzetti L, de Pasquale F, Di Pompeo F, et al. Adding dynamics to the Human Connectome Project with MEG. *NeuroImage*. 2013:80:190–201.

Ma Q, Rolls ET, Huang C-C, Cheng W, Feng J. Extensive cortical functional connectivity of the human hippocampal memory system. *Cortex*. 2022:147:83–101.

Michalareas G, Vezoli J, van Pelt S, Schoffelen JM, Kennedy H, Fries P. Alpha-Beta and Gamma rhythms subserve feedback and feedforward influences among human visual cortical areas. *Neuron*. 2016:89:384–397.

Panzeri S, Rolls ET, Battaglia F, Lavis R. Speed of feedforward and recurrent processing in multilayer networks of integrate-and-fire neurons. *Network*. 2001:12:423–440.

Razi A, Seghier ML, Zhou Y, McColgan P, Zeidman P, Park HJ, Sporns O, Rees G, Friston KJ. Large-scale DCMs for resting-state fMRI. *Netw Neurosci*. 2017:1:222–241.

Renart A, Parga N, Rolls ET. Associative memory properties of multiple cortical modules. *Network*. 1999a:10:237–255.

Renart A, Parga N, Rolls ET. Backprojections in the cerebral cortex: implications for memory storage. *Neural Comput*. 1999b:11: 1349–1388.

Renart A, Moreno R, de la Rocha J, Parga N, Rolls ET. A model of the IT-PF network in object working memory which includes balanced persistent activity and tuned inhibition. *Neurocomputing*. 2001: 38–40:1525–1531.

Rolls ET. Neurophysiological mechanisms underlying face processing within and beyond the temporal cortical visual areas. *Philos Trans R Soc Lond B*. 1992:335:11–21.

Rolls ET. *Cerebral cortex: principles of operation*. Oxford: Oxford University Press; 2016.

Rolls ET. The storage and recall of memories in the hippocampo-cortical system. *Cell Tissue Res*. 2018:373:577–604.

Rolls ET. Learning invariant object and spatial view representations in the brain using slow unsupervised learning. *Front Comput Neurosci*. 2021:15:686239.

Rolls ET. *Brain computations and connectivity*. Oxford: Oxford University Press; 2023a.

Rolls ET. Emotion, motivation, decision-making, the orbitofrontal cortex, anterior cingulate cortex, and the amygdala. *Brain Struct Funct*. 2023b:228:1201–1257.

Rolls ET. Hippocampal spatial view cells for memory and navigation, and their underlying connectivity in humans. *Hippocampus*. 2023c:33:533–572.

Rolls ET. Hippocampal spatial view cells, place cells, and concept cells: view representations. *Hippocampus*. 2023d:33:667–687.

Rolls ET, Deco G. Networks for memory, perception, and decision-making, and beyond to how the syntax for language might be implemented in the brain. *Brain Res*. 2015:1621:316–334.

Rolls ET, Webb TJ, Deco G. Communication before coherence. *Eur J Neurosci*. 2012:36:2689–2709.

Rolls ET, Deco G, Huang C-C, Feng J. The human language effective connectome. *NeuroImage*. 2022a:258:119352.

Rolls ET, Deco G, Huang CC, Feng J. The effective connectivity of the human hippocampal memory system. *Cereb Cortex*. 2022b:32: 3706–3725.

Rolls ET, Deco G, Huang C-C, Feng J. *The connectivity of the human frontal pole cortex, and a theory of its involvement in exploit vs explore*; 2023a.

Rolls ET, Deco G, Huang C-C, Feng J. Human amygdala compared to orbitofrontal cortex connectivity, and emotion. *Prog Neurobiol*. 2023b:220:102385.

Rolls ET, Deco G, Huang C-C, Feng J. Multiple cortical visual streams in humans. *Cereb Cortex*. 2023c:33:3319–3349.

Rolls ET, Deco G, Huang CC, Feng J. The human orbitofrontal cortex, vmPFC, and anterior cingulate cortex effective connectome: emotion, memory, and action. *Cereb Cortex*. 2023d:33:330–359.

Rolls ET, Deco G, Huang CC, Feng J. The human posterior parietal cortex: effective connectome, and its relation to function. *Cereb Cortex*. 2023e:33:3142–3170.

Rolls ET, Deco G, Huang CC, Feng J. Prefrontal and somatosensory-motor cortex effective connectivity in humans. *Cereb Cortex*. 2023f:33:4939–4963.

Rolls ET, Feng R, Cheng W, Feng J. Orbitofrontal cortex connectivity is associated with food reward and body weight in humans. *Soc Cogn Affect Neurosci*. 2023:18:nsab083.

Rolls ET, Feng R, Feng J. Lifestyle risks associated with brain functional connectivity and structure. *Hum Brain Mapp*. 2023:44:2479–2492. https://doi.org/10.1002/hbm.26225.

Rolls ET, Rauschecker JP, Deco G, Huang CC, Feng J. Auditory cortical connectivity in humans. *Cereb Cortex*. 2023:33:6207–6227.

Rolls ET, Wirth S, Deco G, Huang C-C, Feng J. The human posterior cingulate, retrosplenial and medial parietal cortex effective connectome, and implications for memory and navigation. *Hum Brain Mapp*. 2023:44:629–655.

Smith SM. Fast robust automated brain extraction. *Hum Brain Mapp*. 2002:17:143–155.

Smith RE, Tournier JD, Calamante F, Connelly A. SIFT2: enabling dense quantitative assessment of brain white matter connectivity using streamlines tractography. *NeuroImage*. 2015:119:338–351.

Sulpizio V, Galati G, Fattori P, Galletti C, Pitzalis S. A common neural substrate for processing scenes and egomotion-compatible visual motion. *Brain Struct Funct*. 2020:225:2091–2110.

Valdes-Sosa PA, Roebroeck A, Daunizeau J, Friston K. Effective connectivity: influence, causality and biophysical modeling. *NeuroImage*. 2011:58:339–361.

Van Essen DC, Glasser MF. Parcellating cerebral cortex: how invasive animal studies inform noninvasive mapmaking in humans. *Neuron*. 2018:99:640–663.

Wallis G, Rolls ET. Invariant face and object recognition in the visual system. *Prog Neurobiol*. 1997:51:167–194.

Wan Z, Rolls ET, Cheng W, Feng J. Brain functional connectivities that mediate the association between childhood traumatic events and adult mental health and cognition. *EBioMedicine*. 2022:79:104002.

Yokoyama C, Autio JA, Ikeda T, Sallet J, Mars RB, Van Essen DC, Glasser MF, Sadato N, Hayashi T. Comparative connectomics of the primate social brain. *NeuroImage*. 2021:245:118693.

Zhang R, Rolls ET, Cheng W, Feng J. *Different cortical connectivities in human females and males relate to differences in strength and body composition, reward and emotional systems, and memory*; 2023 in review.